[11] Vaglio-Laurin, R. et al., "Supersonic Flow About General Three-Dimensional Blunt Bodies," TR ASD-TR-61-727, Volumes umes I, II, and III, Oct. 1962, General Applied Science Lab., Westbury, N.Y.

[12] Thommen, H. U. and D'Attorre, L., "Calculation of Steady, Three-Dimensional Supersonic Flow Fields by a Finite Difference Method," AIAA Paper 65-26, New York, 1965.

[13] Chu, C. W., Niemann, A. F., and Powers, S. A., "Calculation of Multiple Rocket Engine Exhaust Plumes by the Method of Characteristics, Part I," AIAA Paper 66-651, Colorado Springs, Colo., 1966.

[14] Rakich, J. V., "Three-Dimensional Flow Calculation by the Method of Characteristics," *AIAA Journal*, Vol. 5, No. 10, Oct. 1967, pp. 1906–1908.

[15] Butler, D. S., "The Numerical Solution of Hyperbolic Systems of Partial Differential Equations in Three Independent Variables," *Proceedings of the Royal Society, Series A*, Vol. 255, 1960, pp. 232–252.

[16] Thompson, H. D., Ransom, V. H., and Hoffman, J. D., "An Analytical Study of the Scramjet Exhaust Expansion System," AFAPL-TR-67-142, Pt. I, Nov. 1967, Air Force Aero Propulsion Lab., Wright-Patterson Air Force Base, Ohio.

[17] Elliott, L. A., "Shock Fronts in Two-Dimensional Flow," *Proceedings of the Royal Society, Series A*, Vol. 267, 1962, pp. 558–565.

[18] Richardson, D. J., "The Solution of Two-Dimensional Hydrodynamic Equations by the Method of Characteristics," *Fundamental Methods in Hydrodynamics*, Vol. III, *Methods in Computational Physics*, edited by B. Alder, S. Fernbach, and M. Rotenberg, Academic Press, New York, 1964, pp. 295–318.

[19] Heie, H. and Leigh, D. C., "Numerical Stability of Hyperbolic Equations in Three Independent Variables," *AIAA Journal*, Vol. 3, No. 6, June 1965, pp. 1099–1103.

[20] Darwell, H. M. and Trubridge, F. P., "Design of Rocket Nozzles to Reduce Gas Misalignment," *Journal of Spacecraft and Rockets*, Vol. 6, No. 1, Jan. 1968, pp. 36–41.

APRIL 1970 J. SPACECRAFT VOL. 7, NO. 4

Boundary-Layer Analysis of Low-Density Nozzles, Including Displacement, Slip, and Transverse Curvature

DAVID L. WHITFIELD*
ARO Inc., Arnold Air Force Station, Tenn.

AND

CLARK H. LEWIS†
Virginia Polytechnic Institute, Blacksburg, Va.

Boundary layers in low-density supersonic and hypersonic conical and contoured axisymmetric nozzles were investigated theoretically and comparisons have been made with available experimental data. The nozzle flow conditions treated were such that a thick laminar boundary layer existed on the wall and a small inviscid isentropic core existed along the center line. The nonsimilar laminar boundary-layer equations including first-order transverse curvature terms for internal (nozzle) flow were solved numerically with and without wall slip and temperature jump boundary conditions and boundary-layer displacement effects. Solutions are presented for five low-density nozzles whose exit conditions ranged in Mach number from about 3.0 to 10.0 and in *Re*/ft from about 350 to 15,000. Displacement and transverse curvature effects were significant; however, slip effects were found to be negligible. Agreement between numerical results and experimental data is good, particularly in the nozzle test sections.

Nomenclature

c_p = constant-pressure specific heat
g = total enthalpy ratio, H/H_o
H_o = total enthalpy in reservoir
h = $-q_w/(T_{aw} - T_w)$, heat-transfer coefficient
k = thermal conductivity
L = reference body length
M = Mach number
P, P_o, P'_o = static, total, and Pitot pressures, respectively
Pr = $\mu c_p/k$, Prandtl number
q_w = nozzle wall heat-transfer rate per unit area
R = converging section radius of curvature
Re = $\rho u/\mu$, Reynolds number per unit length
r = radius defined by Eq. (1)
r_w, r^* = nozzle wall and throat radii, respectively
St = $-q_w/\rho_e u_e H_o(1-g_w)$, Stanton number
T, T_0 = static and total temperatures, respectively
$T(0)$ = slip temperature at the wall
T_0' = total temperature behind a normal shock
T_{aw} = adiabatic wall temperature
u = velocity component in x direction
$u(0)$ = slip velocity at the wall
x = surface distance along nozzle wall
y = distance normal to nozzle wall
z = distance along nozzle axis
z_m = total distance along nozzle axis
α = nozzle wall angle
β = $(2\xi/u_e)du_e/d\xi$, dimensionless velocity gradient
δ = boundary-layer thickness (y where $u/u_e = 0.995$)
δ^* = displacement thickness
γ = ratio of specific heats
λ = mean free path

Presented as AIAA Paper 69-653 at the AIAA Fluid and Plasma Dynamics Conference, San Francisco, Calif., June 16–18, 1969; submitted May 5, 1969; revision received October 22, 1969. This work was sponsored by the Arnold Engineering Development Center (AEDC), Air Force Systems Command, U.S. Air Force under Contract F40600-69-C-0001 with ARO Inc., Contract Operator, AEDC. The authors gratefully acknowledge the following ARO Inc. personnel for assistance in performing this research: J. L. Potter and W. H. Carden, for permission to use some of their unpublished numerical results and W. Stephenson for permission to use unpublished viscous correction data for some of the Pitot pressure measurements.

* Engineer, Plume Test and Analysis Section, Testing and Development Branch, Aerospace Environmental Facility.

† Associate Professor of Aerospace Engineering; previously Supervisor, Theoretical Gas Dynamics Section, Hypervelocity Branch, Aerophysics Division, von Kármán Gas Dynamics Facility. Associate Fellow AIAA.

μ = viscosity
ξ = $\int_0^x \mu_e \rho_e u_e (r_w^2/L^2) dx$, transformed surface distance
ρ = mass density of gas

Subscripts

ℓ, E, w = nozzle center line, exit, and wall
e = edge of isentropic core
0 = reservoir conditions

Introduction

THE design and analysis of low-density nozzles have received some attention in recent years.[1-4] Nozzle design is usually accomplished by applying a boundary-layer correction to some desired inviscid flow. One such method is due to Potter and Durand,[2] which was recently modified by Potter and Carden.[3] This method is based on an integral technique which uses the similar solutions of Cohen and Reshotko.[5] The results given by this method have proved to be very useful in designing a nozzle for a particular test section condition. However, a problem frequently arising in practice is that of determining the flow conditions which might be expected from an existing or proposed nozzle. Similar boundary-layer solutions are not applicable for such an investigation since similarity cannot be satisfied in general for any specified set of reservoir conditions, nozzle geometry, and wall temperature distribution. Furthermore, due to the lack of any completely satisfactory correlation parameters, it is difficult to use experimental data from one nozzle to predict reliably how another will operate.

This paper presents the results of a numerical method for the prediction of boundary layers in axisymmetric nozzles with specified reservoir conditions, nozzle geometry, and wall temperature distribution, including the effects of first-order transverse curvature (TVC),[6] velocity slip and temperature jump (STJ),[7] and displacement (DISP), without the restriction of similar boundary-layer theory. The effects of DISP were treated by iterating upon the inviscid and viscous flow fields until there was negligible change in the axial pressure distribution along the nozzle. The nozzle flow conditions treated were such that a thick laminar boundary layer existed on the nozzle wall and a relatively small inviscid isentropic core existed along the center line. Results are presented for five nozzles which have been in operation at the Arnold Engineering Development Center (AEDC).

Numerical Procedure

The coordinate system used herein for internal (nozzle) flow is illustrated in Fig. 1. This coordinate system differs from that for external flow in the definition of the term $r(x,y)$, which for internal flow is defined as

$$r(x,y) = r_w(x) - y \cos\alpha \quad (1)$$

The nonsimilar laminar boundary-layer equations including first-order TVC terms for internal flow are considered in detail in Ref. 8. (In Refs. 6 and 8 first-order TVC, as used herein, is referred to as second-order TVC.) These equations were solved by the basic numerical method developed by Jaffe, Lind, and Smith[6] with modifications made by Mayne, Gilley, and Lewis[7] to include slip and temperature jump at the wall.

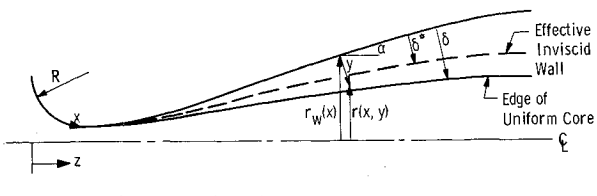

Fig. 1 Nozzle coordinate system.

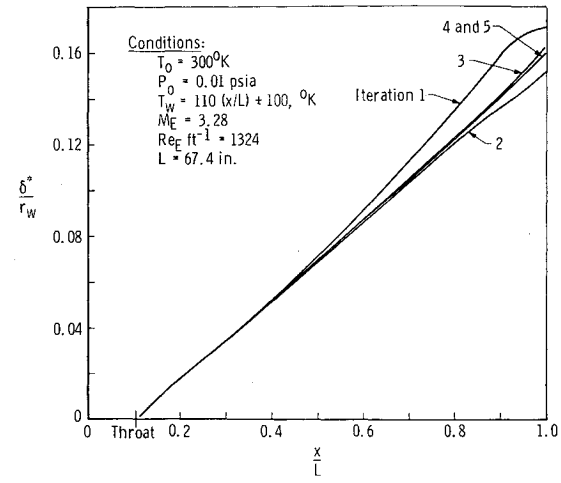

Fig. 2 Displacement thickness for successive iterations in the M3-A nozzle.

The boundary-layer solutions were started at the entrance of the converging portion of the nozzles where u_e was zero, and the procedure was self starting from the known reservoir conditions. The step size along the x coordinate (along the wall) was varied throughout the nozzle depending on the anticipated pressure gradient at a particular point in the nozzle. For example, usually 30–50% of the total number of stations used were located within 2 to 3 throat diameters of the nozzle throat. No difficulty was encountered in obtaining solutions in the throat region of the nozzles.

The data required for computation were: P_o, H_o, $T_w(x)$, Pr, nozzle geometry, and some initial estimation of $P(z)$, the pressure distribution along the axis. Since a given flow through a nozzle will establish its own $P(z)$ for each set of P_o, H_o and $T_w(x)$, the final $P(z)$ was obtained as part of the solution. This solution was accomplished by iteration in the following way: From the displacement thickness δ^* calculated at each station, an effective inviscid area was calculated using the corresponding wall radius. Taking the ratio of this effective area to the throat area, a new $P(z)$ was calculated from one-dimensional perfect gas ($\gamma = 1.4$) expansion theory. The resulting $P(z)$ was then used as the next approximation to the $P(z)$, and the process was repeated until $P(z)$ converged within prescribed accuracy. This iteration process is illustrated in Fig. 2.

Iterations 1 and 3 in Fig. 2 were obtained using a $P(z)$ corresponding to a more highly expanded gas than the $P(z)$ used to obtain iteration 2. This oscillation about the final converged $P(z)$ existed for all solutions where DISP was included. In all cases, the more favorable pressure gradient distributions yielded the larger values of δ and δ^*, since both varied as M^a/Re^b, where $a > 0$ and $b > 0$, for all solutions obtained.

Because of the strong dependence of δ and δ^* on the magnitude of $P(z)$ and hence Re, special attention was given to the initial estimation of $P(z)$, particularly for the low P_E hypersonic nozzles where the boundary layers were very thick, for the following reason: If the initial $P(z)$ used were to correspond to that obtained by taking $\delta^* = 0$, i.e., in the absence of a boundary layer, then the first iteration using this $P(z)$ would give values of δ and δ^* much larger than the final converged values as pointed out in the paragraph before and illustrated in Fig. 2. Therefore, if the nozzle actually operated with a thick boundary layer, as in a very rarefied flow, the first iteration might indicate that the flow had merged. For this reason, the so-called "zeroth" iteration[7] corresponding to a $P(z)$ calculated by neglecting DISP, i.e., $\delta^* = 0$, is in general not an acceptable starting procedure for nozzle flow. Moreover, it was better to be conservative in the initial estimation of $P(z)$, and when possible a less favorable pressure distribution was used than actually existed in the nozzle considered.

Table 1 Nozzles and operating conditions[a]

	M3-A	M3-B[b]	Carden's	M9	M10
P_o, psia	0.002–0.029	0.001–0.029	17.79	30.9	18.3
T_0, °K	300–900	300–900	3370	2475	3100
T_w, °K	110(x/L) + 100	89	333	333	333
M_E	2.60–3.50	2.76–3.80	5.20	9.30	10.15
Re_E/ft	100–3650	38–3000	6200	15000	4660
$(\lambda_w)_E$, in.	0.049–0.364	0.025–0.234	0.002	0.036	0.112
r_E, in.	15.0	15.0	0.62	2.407	3.833
r^*, in.	5.33	5.33	0.103	0.07343	0.07405
L, in.	67.4	67.4	3.68	17.34	19.62
z_m, in.	64.0	64.0	3.0	16.7	18.67
Geometry	Conical (α = 10°)	Conical (α = 10°)	Conical (α = 15°)	Contoured	Contoured

[a] Nitrogen was the test gas used in all nozzles.
[b] Original Mach three nozzle was modified to give better and more uniform wall cooling.

All the solutions calculated were for nitrogen, the test gas used in the particular nozzle experiments considered. The expression used for viscosity in all the calculations was Sutherland's Law, and the Prandtl number used was 0.7068 (constant). All calculations were made on a Control Data Corporation 1604B digital computer.

Experimental Conditions

The conditions for the five nozzles considered are given in Table 1. The Mach 3 nozzles (M3-A and M3-B) were operated in the Aerospace Environmental Facility (AEF) at AEDC and the other three nozzles (M9, M10, and Carden's) were operated in the von Kármán Facility (VKF) at AEDC. Available experimental data from these nozzles consist of P'_o distributions,[3,8] relative heat flux,[3] and nozzle wall heat-transfer coefficients.[4] These five nozzles provided an excellent test for the numerical results because they provided wide ranges in M and Re/ft, constant and variable wall temperature distributions, very thick boundary layers, up to $\delta/r_w = 0.90$, very strong pressure gradients (a static pressure drop of over 3 orders of magnitude in less than 2 in.), and sufficiently rarefied flow to produce some effects of STJ. It might also be pointed out that solutions have been obtained for a subsonic nozzle and a hypervelocity Mach 18 nozzle; however, due to lack of experimental data these results are not discussed herein.

The Mach 3 nozzles, M3-A and M3-B have identical geometry but different wall temperature distributions. Both were operated in the ARC (8V) Vacuum Chamber in AEF. The 8V is a cryogenic chamber using liquid nitrogen (LN_2), gaseous He, and, if necessary, LHe, to maintain a chamber pressure during a run of 10^{-4} to 10^{-5} mm Hg depending on the mass flow rate through the nozzle. The chamber operation was continuous; however, the cryopanels in the chamber had to be brought up to room temperature every few hours to release the condensed gases on their surfaces. The walls of both nozzles were cooled with LN_2 to reduce the boundary-layer growth, but the cooling arrangements differed. The M3-A nozzle had an LN_2 cooling jacket in the throat region, and then LN_2 was forced through copper tubing wrapped around the remaining downstream portion of the nozzle. This arrangement produced a wall temperature distribution that could be closely approximated by $T_w = 110\ (x/L) + 100$, °K. On the M3-B nozzle, an LN_2 jacket was used in place of the copper tubing. This resulted in a uniform, constant T_w of 89°K, a reduction of 121°K at the nozzle exist. The exit Mach number was increased by about 10% at $P_o = 0.01$ psia and $T_0 = 300$°K due to the colder wall.

The designs, operating conditions, and pumping systems of the Carden's, M9, and M10 nozzles have been discussed in detail elsewhere.[3,4] These three nozzles differ from the M3 nozzles primarily in the type of pumping system used and in the fact that an arc heater was used to produce the high total enthalpies required, whereas resistance heaters sufficed to produce the H_o's required for the M3 nozzles. The technique Carden used to measure local heat-transfer coefficients is discussed in Ref. 4. A brief discussion of the method used to measure relative heat flux is given in Ref. 3. A continuous distribution of P_o' in the M9 nozzle was measured by connecting the Pitot probe to a linear potentiometer, which in turn was connected to an x-y plotter along with the signal from the Pitot probe pressure transducer. Thus, it was possible to produce a continuous trace of P_o' data as a function of position rather than discrete points.

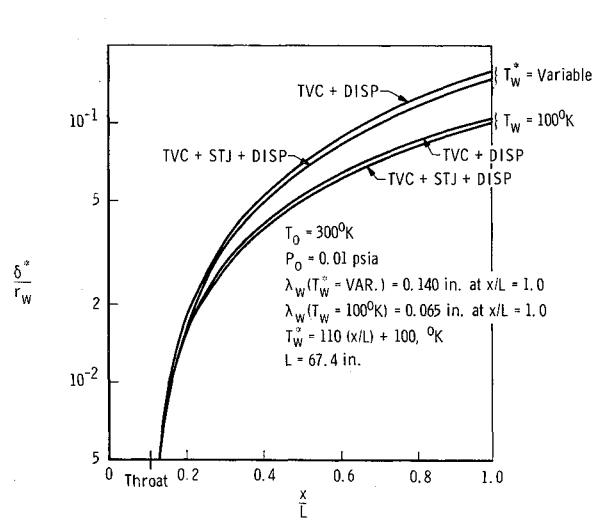

Fig. 3 Displacement thicknesses in the M3-A and M3-B nozzles.

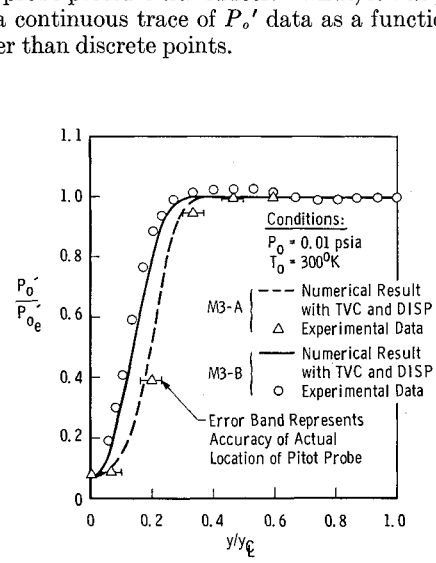

Fig. 4 Calculated and measured Pitot pressure distributions at exit of M3-A and M3-B nozzles.

Table 2 Comparison with Carden's experimental data

	Numerical method	Pressure distribution	Higher-order effects	Source
1.	Beckwith and Cohen (local similarities)	Carden[a]	None	Ref. 4
2.	Incremental flat plate	Carden[a]	None	Ref. 4
3.	Jaffe, Lind, and Smith (nonsimilar)	Carden[a]	None	This paper
4.		Iterated[b]	DISP	
5.		Iterated[b]	DISP + TVC + STJ	

[a] One-dimensional expansion for ideal gas ($\gamma = 1.4$).
[b] Iterated viscous-inviscid ideal gas ($\gamma = 1.4$). One-dimensional expansion.

Results and Discussion

Mach Three Nozzles

A comparison of the displacement thickness in the conical M3 nozzle for two different wall temperature distributions, each with and without STJ, is given in Fig. 3. There is slightly more difference between the solutions with and without STJ for the variable wall temperature [$T_w = 100\,(x/L) + 100$, °K] than for the constant wall temperature ($T_w = 100$°K) due to the larger mean free path λ_w near the hotter wall. The λ_w at the nozzle exit was 0.140 in. for the variable $-T_w$ and 0.065 in. for the constant $-T_w$ conditions. For this particular nozzle, reservoir conditions, and wall temperature distributions, the effect of including STJ was to increase M_E less than 1%.

Figure 4 compares calculated and measured Pitot pressure distributions for the M3-A and M3-B nozzles. The measured values for the M3-A were corrected for viscous effects as described in Ref. 8; however, the corrections had little effect on the absolute values of the measurements. For the M3-B, the P_o' measurements were not corrected for viscous effects. The probe carrier used in obtaining the experimental data in the M3-B nozzle was more accurate in positioning than the one used in the M3-A, and an error band representing the probe location is not shown for the M3-B data. The agreement between theory and experimental data in Fig. 4 is good.

Carden's Nozzle

Carden[4] designed a low P_E axisymmetric nozzle to permit measurement of the wall heat-transfer distribution $q_w(x)$. He also used several approximate theories (e.g., Cohen and Reshotko integral method,[9] Beckwith and Cohen local similarity,[10] and Pasqua et al. incremental flat-plate method[11]) to predict the wall heat-transfer coefficient h. A comparison of Carden's experimental data and two of his numerical solutions with numerical results from the present analysis is shown on Fig. 5 and Table 2. Both of Carden's solutions and one from the present analysis used the same one-dimensional perfect gas ($\gamma = 1.4$) expansion theory. The remaining two solutions from the present analysis included the effects of DISP on the one-dimensional inviscid $P(z)$. In comparing the present numerical results with Carden's numerical results based on the same $P(z)$, it is significant that the prediction from the nonsimilar boundary-layer theory falls below both the local similarity and incremental flat-plate predictions. The inclusion of the nonsimilar terms has in all known previously published investigations led to substantial increases in q_w in regions of strong favorable pressure gradients (see e.g., Marvin).[12] However, it is also significant that the predictions of the throat q_w* from both approximate methods used by Carden and shown on Fig. 5 and Table 2 strongly depended upon a reference q_w which was taken near the exit of the nozzle. It will be shown later that q_w, particularly near the nozzle exit, can

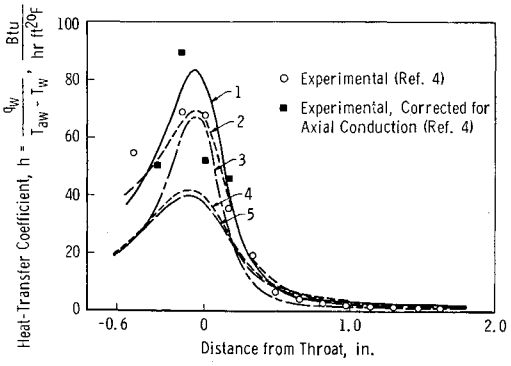

Fig. 5 Calculated and measured heat-transfer coefficients in Carden's nozzle. (See Table 2 for key to theoretical calculations.)

be substantially affected by transverse curvature which was not included in calculating the reference q_w nor in the approximate theories. In comparing the present numerical results with the experimental data, one should note the strong effects of displacement on the numerical results and the large correction for axial conduction on the experimental data in the throat region. Carden[4] discussed a "rough calculation" procedure he used to correct for axial conduction. He also discussed the effects of thermal radiation on the experimental data and the influence of the one-dimensional flow model on the numerical results. The influence of these effects has not been determined. Further experimental and numerical investigations are needed to explain the large differences between the experimental wall heat-transfer data and the numerical predictions.

Figure 6 indicates the effects of STJ and first-order TVC on the Stanton number for Carden's nozzle. Notice that for internal flow, contrary to external flow, the effect of first-order TVC was to decrease rather than increase the Stanton number.

Mach Nine Nozzle

Figures 7 and 8 show good agreement between numerical results and experimental data for the M9 nozzle.[8] The solutions were obtained by approximating the contoured nozzle wall downstream of the throat by a conical wall. The continuous distribution of measured P_o' in Fig. 7 was obtained using a linear potentiometer and an x-y plotter as discussed earlier. No viscous correction was applied to the measured P_o' distribution in Fig. 7 since the correction was less than 2% over most of the boundary layer.[8] In Fig. 8, the discrepancy between measured values of relative heat flux, i.e., T_0'/T_0'₵, and the calculated values of H/H_o, was less than 4%.

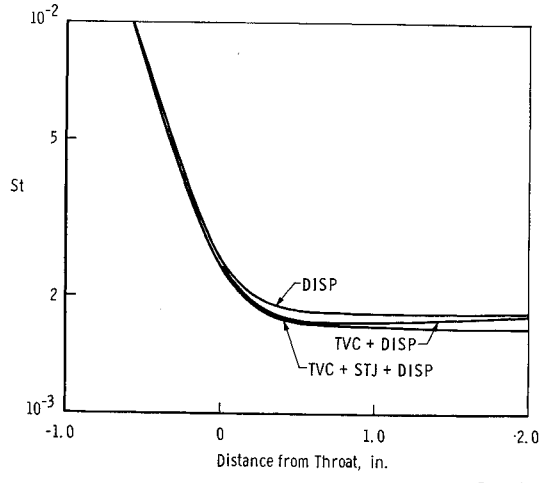

Fig. 6 Calculated Stanton number distribution in Carden's nozzle.

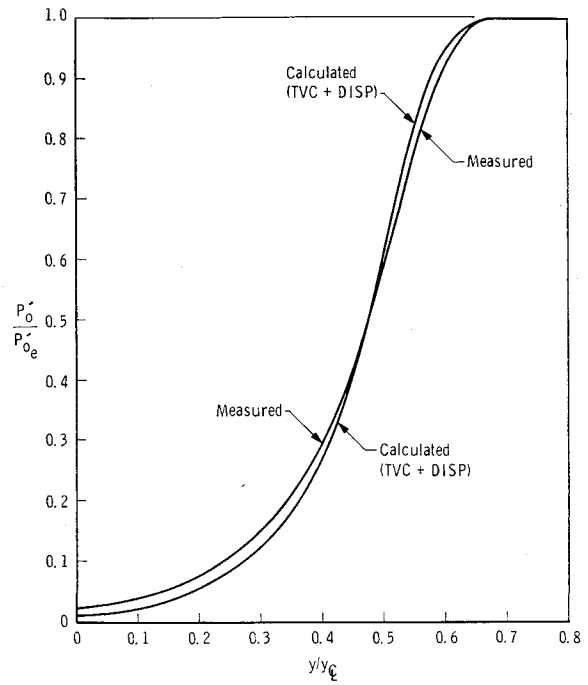

Fig. 7 Calculated and measured Pitot pressure distributions at exit of M9 nozzle.

Figures 9 and 10 show some results of two solutions for the M9 nozzle that indicate the effects of first-order TVC only. These solutions were obtained using the actual contoured nozzle wall. The same $P(z)$ was used for each solution, and the displacement effect was not iterated. Figure 9 indicates the importance of including first-order TVC in the case of a thick boundary layer. The calculated δ_E $(x/L = 1.0)$ shown in Fig. 9 was reduced about 15% when first-order TVC was neglected. For this particular nozzle and operating conditions, the drop in calculated P_o' occurred at the edge of the boundary layer as shown in Fig. 8. If the location of the drop in calculated P_o' in Fig. 7 were displaced 15% by neglecting first-order TVC, then a significant error would be involved in predicting the P_o' distribution. The reduction in q_w resulting from the first-order TVC effect is illustrated in Fig. 10, including first-order TVC reduced q_{wE} by 28%. It should be

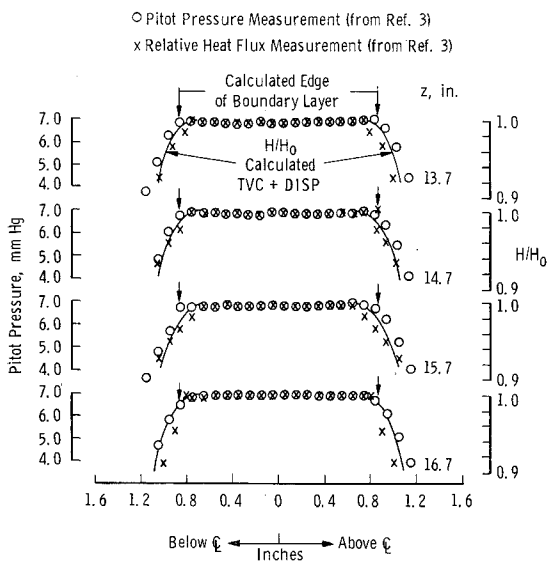

Fig. 8 Calculated total enthalpy distribution, calculated edge of boundary layer, measurements of relative heat flux, and measurements of Pitot pressure in M9 nozzle.

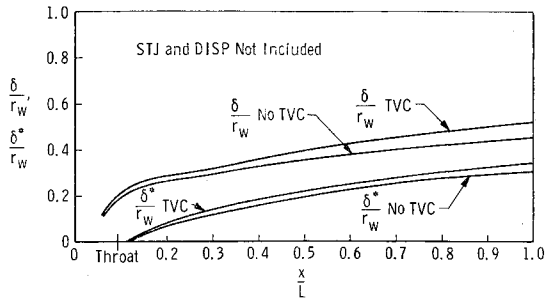

Fig. 9 Boundary-layer and displacement thickness in contoured M9 nozzle with and without TVC.

pointed out that inclusion of DISP and STJ will also affect the prediction of $\delta(x)$ and $q_w(x)$.

Figure 11 compares boundary-layer and displacement thicknesses as calculated by the present method and the method of Potter and Carden[8] for the same contoured nozzle and axial pressure distribution. The $P(z)$ used to obtain the results for the numerical comparison in Fig. 11 was that used by Potter and Carden in the design of the nozzle; however, this was not the experimentally measured $P(z)$ that actually existed in the nozzle when it was operated. In order to compare the predicted $P(z)$ in the nozzle using the present method with the actual $P(z)$, a comparison of the calculated δ^*/r_w including DISP with experimental values of δ^*/r_w is made in Fig. 11. It is difficult to completely determine the difference between the two numerical methods based upon the measured $P(z)$. However, in view of the comparison in Fig. 11, the present method including DISP predicts δ and δ^* well for this nozzle.

It is interesting to note that the pressure gradient parameter, β, reached a maximum of about 9 near the throat of this nozzle and dropped to about 0.04 near the exit.[8] Thus similarity solutions (e.g., Cohen and Reshotko[5]) are not applicable‡ for these nozzle flows especially in the throat region. It has been shown by Lewis and Whitfield[18] that a breakdown of similarity in regions of strong favorable pressure gradients can substantially affect the prediction of the boundary-layer growth downstream of the breakdown in similarity.

Mach Ten Nozzle

Figure 12 shows good agreement between calculated and measured P_o' distributions[8] for two locations in the test section of the M10 nozzle. The numerical results in Fig. 12 include the effects of first-order TVC and STJ but not DISP.

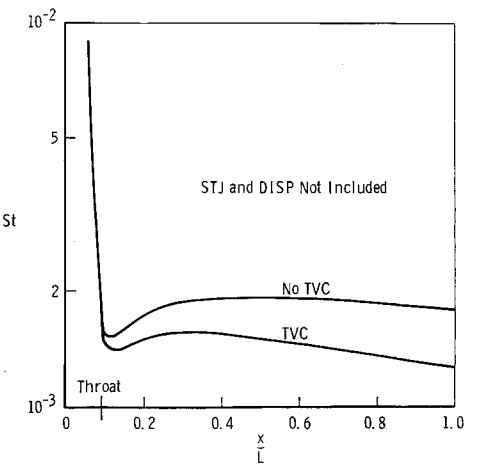

Fig. 10 Heat-transfer distribution in contoured M9 nozzle.

‡ The streamwise variation of some terms which are neglected in similarity solutions is given in Ref. 8.

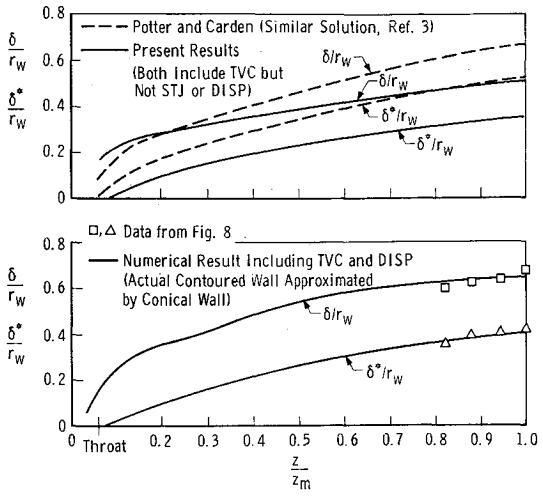

Fig. 11 Numerical and experimental boundary layer and displacement thicknesses in M9 nozzle.

The pressure distribution downstream of the throat which was used in the numerical calculations was obtained by computing the $P(z)$ in a conical inviscid nozzle with $M_E = 10.15$ (the measured M_E). The $P(z)$ upstream of the throat was obtained by using the geometric wall and assuming that the flow in this region was inviscid. This was a good assumption upstream of the throat for this nozzle since δ^* was very small and even negative in the vicinity of the throat due to the cold wall, i.e., $T_w/T_0 \ll 1$. One-dimensional, $\gamma = 1.4$, expansion theory was used to compute $P(z)$ both upstream and downstream of the throat.

Some Effects of Velocity Slip and Temperature Jump

Figures 13 and 14 indicate the magnitude of the velocity slip and temperature jump calculated for the M3-A nozzle, Carden's nozzle, and the M10 nozzle. From Fig. 13 notice that the flow merged, i.e., the boundary layer completely filled the nozzle, for the M3-A and M10 nozzles before a velocity slip of 10% was reached. Notice also from Fig. 13 the M3-A nozzle had the largest amount of velocity slip and in Fig. 14 the M10 nozzle had the largest temperature jump. This was due in part to the difference in the relation between the axial gas static temperature distributions in the nozzles and $T_w(x)$'s. Also, the nature of the gas static temperature profile across the boundary layer was different in each nozzle, and this had significant affect on the calculated temperature jump. To illustrate this effect, consider Fig. 14 where negative values of $[T(0) - T_w]/T_w$ occurred in the M3-A nozzle when T_e/T_w dropped to about 0.8; whereas, for the M10 nozzle, the curve of $[T(0) - T_w]/T_w$ is everywhere positive and monotone increasing and T_e/T_w is below 0.5. These effects are caused by

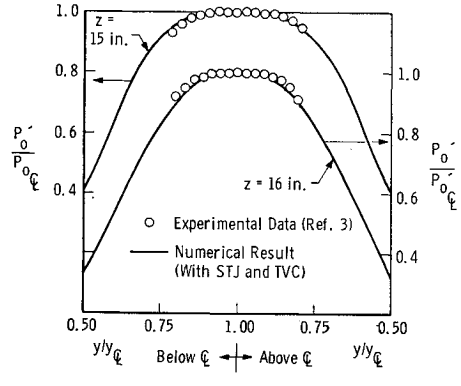

Fig. 12 Calculated and measured Pitot pressure distributions in test section of M10 nozzle.

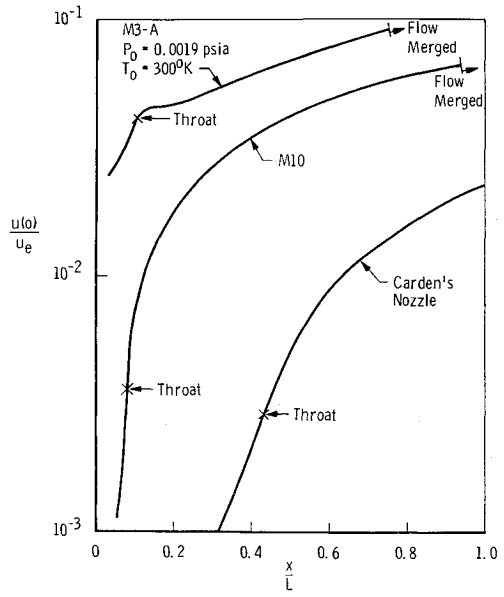

Fig. 13 Velocity slip in M3-A, M10, and Carden's nozzle. (All results with STJ and TVC and without DISP.)

the difference in the slopes of the static temperature profiles in the vicinity of the wall.[8]

Nozzle Design

The aforementioned method was recently extended to design a nozzle for a particular test-section condition. The procedure consisted of specifying the desired $P(z)$, P_o, H_o, Pr, $T_w(x)$, effective inviscid nozzle geometry, and an initial estimate of the actual nozzle geometry. Iteration was then performed on $r_w(x)$ instead of on the $P(z)$ as was the case for analyzing the boundary layer in a specified nozzle. Each successive approximation to $r_w(x)$ in the iteration process was obtained by adding $\delta^* \cos\alpha$ to the effective inviscid wall radius. The solutions were less sensitive to $r_w(x)$ than to $P(z)$ and convergence was more rapid.

Conclusions

The first-order (Prandtl) boundary-layer equations, modified to include first-order transverse curvature (TVC) and velocity slip and temperature jump (STJ) terms and including the effects of displacement, were applied to low-density supersonic and hypersonic nozzle flows and results were compared with experimental data. The major conclusions were as follows:

1) The method well predicts boundary-layer (δ) and boundary-layer displacement (δ^*) thickness distributions along the nozzles, Pitot pressure and stagnation temperature distributions normal to the nozzle axis, and nozzle exit conditions.

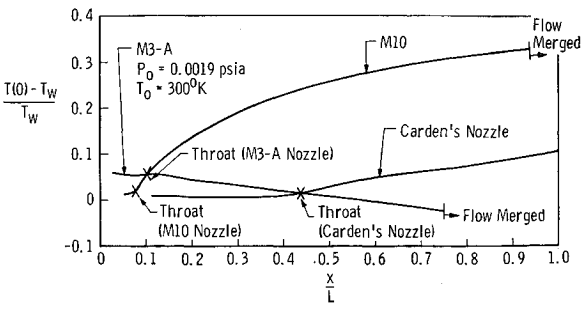

Fig. 14 Temperature jump in M3-A, M10, and Carden's nozzle. (All results with STJ and TVC and without DISP.)

2) TVC had a significant effect on δ and δ^*, especially near the nozzle exit where the effect was as large as 15%.

3) Predictions of wall heat-transfer rate were not as good as those of earlier methods. However, the earlier methods were more approximate, involved arbitrarily defined reference quantities, and predicted about the same heat-transfer rate as the present method when no higher-order effects were included, and fortuitous agreement was obtained with the experimental data. More experimental investigation is needed.

4) Effects of a variable wall temperature distribution were larger than the effects of STJ.

5) The method has been successfully applied to a nozzle where δ is 90% of the nozzle radius. The method can therefore be applied so long as an inviscid core exists, even though the size of the inviscid core is only 1% of the cross-sectional area of the nozzle.

References

[1] Petrie, S. L., "Boundary Layer Studies in an Arc-Heated Tunnel," CR-96152, 1968, NASA.

[2] Potter, J. L. and Durand, J. A., "Analysis of Very Thick Laminar Boundary Layers in Axisymmetric High-Speed Fluid Flow," *Development in Theoretical and Applied Mechanics*, Plenum Press, New York, 1963, pp. 341–360.

[3] Potter, J. L. and Carden, W. H., "Design of Axisymmetric Contoured Nozzles for Laminar Hypersonic Flow," *Journal of Spacecraft and Rockets*, Vol. 5, No. 9, Sept. 1968, pp. 1095–1100.

[4] Carden, W. H., "Local Heat-Transfer Coefficients in a Nozzle with High-Speed Laminar Flow," *AIAA Journal*, Vol. 3, No. 12, Dec. 1965, pp. 2183–2188; also AEDC-TDR-64-61, April 1964, Arnold Engineering Development Center.

[5] Cohen, C. B. and Reshotko, E., "Similar Solutions for the Compressible Laminar Boundary Layer with Heat Transfer and Pressure Gradient," Rept. 1293, 1956, NACA.

[6] Jaffe, N. A., Lind, R. C., and Smith, A. M. O., "Solution to the Binary Diffusion Laminar Boundary Layer Equations Including the Effect of Second-Order Transverse Curvature," *AIAA Journal*, Vol. 5, No. 9, Sept. 1967, pp. 1563–1569.

[7] Mayne, A. W., Gilley, G. E., and Lewis, C. H., "Binary Boundary Layer on Sharp Cones in Low Density Supersonic and Hypersonic Flow," *AIAA Journal*, Vol. 7, No. 4, April 1969, pp. 699–706.

[8] Whitfield, D. L., "Theoretical and Experimental Investigation of Boundary Layers in Low-Density Hypersonic Axisymmetric Nozzles," TR-68-193, 1968, Arnold Engineering Development Center.

[9] Cohen, C. B. and Reshotko, E., "The Compressible Laminar Boundary Layer with Heat Transfer and Arbitrary Pressure Gradient," Rept. 1294, 1956, NACA.

[10] Beckwith, I. E. and Cohen, N. B., "Application of Similar Solutions to Calculation of Laminar Heat Transfer on Bodies with Yaw and Large Pressure Gradient in High-Speed Flow," TND-625, 1961, NASA.

[11] Pasqua, P. F. et al., "Analytical Studies on Nozzle Throat Cooling," AEDC-TDR-63-58, 1963, Arnold Engineering Development Center.

[12] Marvin, J. G. and Sinclair, A. R., "Convective Heating in Regions of Large Favorable Pressure Gradient," *AIAA Journal*, Vol. 5, No. 11, Nov. 1967, pp. 1940–1948.

[13] Lewis, C. H. and Whitfield, J. D., "Theoretical and Experimental Studies of Hypersonic Viscous Effects," AGARDOgraph 97, Pt. III, May 1965; also AEDC-TR-65-100, May 1965, Arnold Engineering Development Center.